



Simulating ozone dry deposition at a boreal forest with a multi-layer canopy deposition model

Putian Zhou¹, Laurens Ganzeveld², Üllar Rannik¹, Luxi Zhou^{1, *}, Rosa Gierens¹, Ditte Taipale^{3,4}, Ivan Mammarella¹, and Michael Boy¹

¹University of Helsinki, Department of Physics, P.O. Box 64, FI-00014, University of Helsinki, Finland

²Wageningen UR

³University of Helsinki, Department of Forest Sciences, P.O. Box 27, FI-00014, University of Helsinki, Finland

⁴Estonian University of Life Sciences, Department of Plant Physiology, Kreutzwaldi 1, EE-51014, Estonia

* now at U.S. Environmental Protection Agency, Research Triangle Park, NC, USA

Correspondence to: Zhou Putian (putian.zhou@helsinki.fi)

Abstract. A multi-layer ozone (O₃) dry deposition model has been implemented into SOSAA (a model to Simulate the concentrations of Organic vapours, Sulphuric Acid and Aerosols) to improve the representation of O₃ within and above the forest canopy in the planetary boundary layer where O₃ is a key oxidant agent of biogenic volatile organic compounds (BVOCs) and thus affecting organic aerosol processes. We aim to predict the O₃ uptake by a boreal forest canopy under varying environmental conditions and analyse the influence of different factors on total O₃ uptake by the canopy as well as the vertical distribution of deposition sinks inside the canopy.

We evaluated the newly implemented canopy deposition model by an extensive comparison of simulated and observed O₃ fluxes and concentration profiles within and above the boreal forest canopy at SMEAR II (the Station to Measure Ecosystem-Atmosphere Relation II) in Hyytiälä, Finland, in August, 2010. The first half of August showed extremely warm and dry conditions which were probably representative for summer conditions prevailing at this site in future. The simulated O₃ turbulent fluxes at the canopy top and the O₃ concentration profiles inside the canopy agreed well with the measurement, which indicated that the turbulent transport and the O₃ dry deposition onto the canopy and soil surface appeared to be properly represented in the model.

In this model, the fraction of wet surface on vegetation leaves was parameterised according to the ambient relative humidity (RH). Model results showed that when RH was larger than 70% the O₃ uptake onto wet skin contributed 48.6% to the total deposition during nighttime and 22.0% during daytime. In addition, most of the O₃ deposition occurred below 0.8 h_c (canopy height) at this site. The contribution of sub-canopy deposition below 4.2 m was modelled to be about 40% of the total O₃ deposition during daytime which was similar to previous studies. Whereas for nighttime, the simulated sub-canopy deposition contributed 40–65% to the total O₃ deposition which was about two times as that in previous studies (25–30%). The overall contribution of soil uptake was estimated as 36.5%. These results indicated the importance of non-stomatal O₃ uptake processes, especially the uptake on wet skin and soil surface.

Furthermore, a qualitative evaluation of the chemical removal time scales indicated that the chemical removal rate within canopy was about 5% of the total deposition flux at daytime and 16% at nighttime under current knowledge of air chemistry.



The evaluation of the O₃ deposition processes provides improved understanding about the mechanisms involved in the removal of O₃ for this boreal forest site which are also relevant to the removal of other reactive compounds such as the BVOCs and their oxidation products, which will be focus of a follow-up study.

1 Introduction

5 Tropospheric ozone (O₃) is an important oxidant of many reactive species such as biogenic volatile organic compounds (BVOCs) emitted from the forest canopy (Bäck et al., 2012; Smolander et al., 2014). It also plays a significant role in the regulation of the atmospheric oxidation capacity first of all by being one of the primary sources of the hydroxyl radical (OH) which is the most critical oxidant in the air (Mogensen et al., 2015). O₃ also initiates the formation of Criegee intermediate (CI) radicals which are crucial in tropospheric oxidation (Boy et al., 2013). As an air pollutant, O₃ can cause damage to human
10 health (Kampa and Castanas, 2008) and affect ecosystem functioning via its various toxic impacts (Felzer et al., 2007). O₃ can also alter the global radiative forcing as an important greenhouse gas (Stocker et al., 2013, chap. 2). Hence it is important to understand the O₃ budget including its sources and sinks at local or site scale in order to understand the global scale implications.

O₃ is produced via photochemical reactions in the presence of precursor gases, e.g., volatile organic compounds (VOCs), CO
15 (carbon oxide), OH and NO_x (nitric oxide and nitrogen dioxide) or transported downward from stratosphere, and is removed mainly near the Earth's surface. For vegetated surfaces a large part of the removal processes are via stomatal uptake on leaf surface and non-stomatal uptake on plant canopies and soil surface (Wesely, 1989; Ganzeveld and Lelieveld, 1995; Altimir et al., 2006; Rannik et al., 2012; Launiainen et al., 2013), as well as depleted by chemical reactions (Kurpius and Goldstein, 2003; Wolfe et al., 2011). In this study we only focus on the O₃ removal processes, more particularly on the O₃ uptake by
20 boreal forest which covers 33% of global forest land (Ruckstuhl et al., 2008).

For vegetation, the uptake of O₃ depends on the turbulence intensity above and within the canopy, the diffusive transfer in the quasi-laminar boundary layer over the leaf surface, the biological properties of the plants, surface wetness condition, and soil type (Ganzeveld and Lelieveld, 1995). Among them the effect of canopy wetness on O₃ deposition has attracted a lot of attention in previous studies which were also summarised in Massman (2004). For different vegetation types and
25 under different environmental conditions the surface wetness can enhance or reduce O₃ deposition (Massman, 2004). For boreal forest, a number of studies have revealed an enhancement of the O₃ uptake under dew or high humidity conditions. For example, Lamaud et al. (2002) reported that dew on canopy surface significantly increased the O₃ uptake at night and in the morning over a pine stand. Altimir et al. (2006) also found that the condensed moisture on the surfaces enhanced the non-stomatal O₃ uptake in a Scots pine forest when ambient relative humidity (RH) was over 60 - 70%. Similarly to Altimir
30 et al. (2006), Rannik et al. (2012) revealed a strong sensitivity of the nighttime O₃ uptake to RH.

In addition, the boreal forest emits a large portion of BVOCs which are considered to play a significant role in non-stomatal removal of O₃ by oxidation in several studies (Kurpius and Goldstein, 2003; Goldstein et al., 2004; Wolfe et al., 2011). For example, Fares et al. (2010) found the correlation between the oxidation products of monoterpene and O₃ non-stomatal flux at



a ponderosa pine stand in California, US, indicating the gas-phase reactions of O₃ with BVOCs were mostly responsible for O₃ non-stomatal loss. In a model study, Wolfe et al. (2011) suggested that the non-stomatal O₃ uptake at the same Californian site could be explained by considering the role of O₃ destruction with the presence of very reactive BVOCs. Consequently, further analysis of the role of non-stomatal removal of O₃ also strongly depends on the improvement of BVOCs measurement.

5 However, the influence of this gas-phase chemical removal process may vary among different sites. A study by Rannik et al. (2012), who conducted a detailed analysis of a long-term O₃ deposition flux measurement at a boreal forest station in Hyytiälä, Finland, indicated that, at the currently known strength of BVOC emissions, the air chemistry of BVOCs was not likely an important O₃ sink term at this site.

These removal processes altogether determine the contribution of O₃ uptake on forest ground surface and understory vegetation, the vertical distribution of O₃ concentration as well as the non-stomatal uptake contribution, which are considered as three crucial challenges to understand the relationship between the eddy-covariance measurements and O₃ uptake (Launiainen et al., 2013). Therefore several numerical models have been developed to study and simulate O₃ dry deposition processes under different climatic and environmental conditions, which are generally based on the surface deposition model described by Wesely (1989). Among these models, the so-called 'big-leaf' approach method is widely used and usually coupled to regional or global models to estimate the O₃ deposition flux in large scales (e.g. Zhang et al., 2002). However, the 'big-leaf' approach does not consider explicitly the role of in-canopy interactions between biogenic emissions, chemistry, turbulence and deposition. Therefore, more detailed multi-layer models including the role of these in-canopy interactions have been developed and applied to analyse in-canopy deposition-related mechanisms (e.g. Ganzeveld et al., 2002b; Altimir et al., 2006; Rannik et al., 2012; Launiainen et al., 2013). These multi-layer canopy exchange models have also been coupled to large scale models, e.g.,

15 a global chemistry-climate model system (Ganzeveld et al., 2002a), or have been implemented in column models with detailed vertically separated layers (e.g. Wolfe and Thornton, 2011). Recent models have been developed more and more based on the physical, chemical and biological processes under actual environmental conditions, which reduce the dependency of empirical parameters (Wesely and Hicks, 2000).

In this study a multi-layer process-based O₃ dry deposition model was implemented into the 1-dimension (1D) chemical transport model SOSAA (a model to Simulate the concentrations of Organic vapours, Sulphuric Acid and Aerosols). This deposition model was based on the dry deposition representation originally described in Ganzeveld and Lelieveld (1995) and Ganzeveld et al. (1998) and implemented in the Multi-Layer Canopy CHEMistry Exchange Model (MLC-CHEM, manuscript in preparation). This canopy exchange system in MLC-CHEM was already applied in a single column model on the analysis of site-scale exchange processes (Ganzeveld et al., 2002b; Seok et al., 2013), as well as in a global chemistry-climate model system on the analysis of atmosphere-biosphere exchange processes (Ganzeveld et al., 2002a, 2010).

25
30

Furthermore, the long-term continuous measurements and extensive campaigns at SMEAR II have provided a vast amount of data with complementary information on micrometeorology as well as O₃ fluxes and concentrations, which are highly appropriate for validating the new model and also shining a light on those three challenges with the model. We selected a featured month August 2010 for such an extensive evaluation of the model because this month was characterised by exceptional hot and dry conditions in the first two weeks, which possibly represented a future climate at this site (Williams et al., 2011),

35



then followed by two cooler weeks. This study is a starting point of investigating gas dry deposition processes in SOSAA. We aim to evaluate not only quantitatively O₃ fluxes and concentration profiles but also the role of individual deposition processes at this site. This is a prerequisite for a further analysis of BVOCs deposition and chemistry in the follow-up research.

In the following section, a detailed description of the measurement and model will be shown. The comparison and analysis of observed and simulated meteorological quantities, O₃ fluxes, O₃ concentration profiles, chemical removal process and corresponding discussions are described in section 3, followed by a summary in section 4.

2 Methods

2.1 Site

All the measurement data used in this study were from SMEAR II (the Station to Measure Ecosystem-Atmosphere Relation II) located in Hyytiälä, Finland (61°51'N, 24°17'E, 181 m above the sea level) (Hari and Kulmala, 2005). The boreal coniferous forest is relatively homogeneous around the station in all the directions within 200 m, 75% covered by Scots pine (*Pinus sylvestris*) and the rest covered by Norway Spruces (*Picea abies*) and deciduous trees (Bäck et al., 2012). The understory vegetation mainly consists of lingonberry (*Vaccinium vitis-idaea*) and blueberry (*Vaccinium myrtillus*) with a mean height of 0.2 - 0.3 m. The forest floor is covered by dense mosses, mostly *Dicranum polysetum*, *Hylocomium splendens* and *Pleurozium schreberi*. Underneath is a 5 cm layer of humus in soil (Kolari et al., 2006; Kulmala et al., 2008). In 2010, the tree height reaches around 18 m. The all-sided leaf area index (LAI) is about 7.5 m² m⁻², including ~6.0 m² m⁻² overstory vegetation, ~0.5 m² m⁻² understory vegetation and ~1 m² m⁻² moss layer (Launiainen et al., 2013). The vertical profiles of LAI and leaf area density (LAD) are shown in Fig. 1.

2.2 Measurements

The measurement data at SMEAR II are currently publicly available in the data server maintained by AVAA open data publishing platform (<http://avaa.tdata.fi/web/smart/smea>), which was originally introduced in Junninen et al. (2009). A part of observed quantities used in this study are available at 4.2 m, 8.4 m, 16.8 m, 33.6 m, 50.4 m and 67.2 m (above the ground level, the same below), including air temperature (measured by Pt100 sensor), air water content (Li-Cor LI-840 infrared light absorption analyser) and O₃ concentration (TEI 49C ultraviolet light absorption analyser). Other observed quantities include the photosynthetically active radiation (PAR, 400–700 nm) (Li-Cor Li-190SZ quantum sensor) measured at 18 m, PAR (array of 4 Li-Cor Li-190SZ sensors) measured at 0.6 m, net radiation (Reeman MB-1 net radiometer) at 67 m, O₃ flux (Gill Solent HS 1199 sonic anemometer & Unisearch Associates LOZ-3 gas analyzer) at 23 m, friction velocity (Gill Solent 1012R anemometer/themometer) at 23 m, sensible and latent heat fluxes (H and LE) (Gill Solent 1012R and Li-Cor LI-6262 gas analyzer) at 23 m, and soil heat flux (Hukseflux HFP01 heat flux sensors).

In this study the measured O₃ fluxes were calculated over 30 min averaging period using the EddyUH software (Mammarella et al., 2016) and according to standard methodology (for more details see Rannik et al., 2012). Other variables were also half-



hour averaged to fit the model time step for both input and output. The air temperature, RH and O₃ concentration were linearly interpolated using the observations collected at a height of 16.8 m and 33.6 m to arrive at the estimated parameter values at 23 m to allow a direct comparison of the model results with the measurements or being used as input for the model. In addition, some of the observed parameters were also used to constrain the model simulations (see next section).

5 The measured O₃ fluxes were filtered based on the fact that previous studies showed that the measured fluxes had large errors under very low turbulence (Rannik et al., 2006). The threshold of such low turbulence condition was usually set according to the measured friction velocity on top of the canopy in the range of 0.1 m s⁻¹ to 0.25 m s⁻¹ (Altimir et al., 2006; Rannik et al., 2012; Launiainen et al., 2013). Here the observed O₃ fluxes were excluded when $u_* \leq 0.2 \text{ m s}^{-1}$ which was consistent with the study by Rannik et al. (2012). Secondly, the O₃ flux measurements were filtered out when precipitation occurred within
10 preceding 1 hour. Previous studies used a more strictly criteria for such a filter that the preceding 12 hours should keep dry to ensure dry canopy conditions (Altimir et al., 2006; Launiainen et al., 2013). However, in this study the fraction of wet canopy skin was taken into account and consequently we applied the filtering criteria of 1 hour. Overall, 58% of O₃ flux data were available compared to 87% prior to filtering.

2.3 Model description

15 2.3.1 SOSAA

SOSAA is a 1D chemical transport model which couples different modules to simulate the emissions of BVOCs, chemical reactions of organic and inorganic compounds in the air, transportation of trace gases and aerosol particles, as well as the aerosol processes within and above the canopy in the planetary boundary layer. It was first introduced as SOSA by Boy et al. (2011) based on the 1D version of SCADIS (SCAlar DIStribution, Sogachev et al., 2002). After that an aerosol module
20 based on UHMA (University of Helsinki Multicomponent Aerosol model, Korhonen et al., 2004) was implemented by Zhou et al. (2014) resulting in its name being changed to SOSAA. The current version of SOSAA includes five modules. The meteorology module is based on SCADIS. Emissions of BVOCs from the canopy are calculated by the Model of Emissions of Gases and Aerosols from Nature (MEGAN, Guenther et al., 2006). The Master Chemical Mechanism (MCM) v3.2 (<http://mcm.leeds.ac.uk/MCM>) has been implemented to provide chemistry information. The nucleation, condensation, coagulation
25 and deposition of aerosol particles are described by UHMA. In this study a gaseous compound dry deposition module has been implemented into SOSAA. SOSAA has already been applied and verified in several studies (e.g., Kurtén et al., 2011; Mogensen et al., 2011; Boy et al., 2013; Mogensen et al., 2015; Bäck et al., 2012; Smolander et al., 2014; Zhou et al., 2015).

SOSAA is partly constrained by SMEAR II measurements and ERA-Interim reanalysis dataset provided by the European Centre for Medium-Range Weather Forecasts (ECMWF, Dee et al., 2011). The prognostic variables air temperature, horizontal
30 wind speed and specific humidity near and within the canopy are nudged to local measurement data at every time step. In addition, the measurement data of soil heat flux, the incoming direct and diffuse radiations, along with the incoming long wave radiation are read in to modify the set-up of the system in order to simulate a realistic representation of the micrometeorology. It should be noted that the upward radiation at the canopy top, including the reflected and scattered short wave radiation as well



as the emitted long wave radiation, is explicitly computed as a function of canopy structure parameters in SOSAA. The upward radiation is then used to calculate the net radiation on top of the canopy. The upper boundary conditions of air temperature, horizontal wind speed and specific humidity are constrained by the reanalysis datasets. All the input data are interpolated to match the model time for each time step.

5 2.3.2 Multi-layer O₃ dry deposition model

A gas dry deposition model has been implemented into SOSAA to investigate the influence of the dry deposition processes on the atmosphere-biosphere gas exchange and in-canopy gas concentrations. In this study we focus on the O₃ dry deposition since it is the basis of calculating the uptake of other trace gases, including BVOCs (Wesely, 1989). In this multi-layer dry deposition model the O₃ deposition flux is calculated at each layer as

$$10 \quad F_i = [\text{O}_3]_i \cdot V_{d,i} \quad (i = 1, \dots, N) \quad (1)$$

where F is the O₃ deposition flux (ppbv m s⁻¹), $[\text{O}_3]$ is the O₃ concentration (ppbv), V_d is the deposition velocity (m s⁻¹). The subscript i represents layer index. Layer 1 is the bottom layer including the soil surface and the understory vegetation where the moss layer is considered as part of the soil surface for simplicity. The overstory layers 2 to N include only vegetation surface, where N is the layer index at the canopy top.

15 V_d is calculated for bottom layer (layer 1) and overstory layers (layers 2 to N) differently. In addition, the deposition onto dry and wet parts of the leaf surface is considered separately. In overstory layers, only the deposition onto leaves is taken into account, while in the bottom layer the additional pathway of deposition onto the soil surface exists. Thus

$$V_{d,i} = \frac{\text{LAI}_i}{r_{veg,i}} + \frac{\delta_{i1}}{r_{soil} + r_{ac}} \quad (2)$$

20 where LAI_i is the all-sided leaf area index for each layer (m² m⁻²), r_{veg} is the leaf surface resistance (s m⁻¹, the unit is the same for the resistances shown below), r_{soil} (= 600 s m⁻¹) is the soil resistance. The default value 400 s m⁻¹ of r_{soil} applied in Ganzeveld and Lelieveld (1995) is representative for global scale studies, turning out to result in too large soil removal in the simulations of this study. Hence a larger resistance value (600 s m⁻¹) has been applied here. r_{ac} is the resistance representing the turbulent transport from the reference height of the understory vegetation to the soil surface. Since the gas transport is explicitly calculated in SOSAA and the bottom layer height is only ~0.3 m, the turbulence resistance between vegetation and
 25 ground is expected not to be an important factor for soil deposition, and consequently we have set r_{ac} to a very small value (1 s m⁻¹). The Kronecker delta δ_{i1} ($\delta_{i1} = 1$ when $i = 1$; $\delta_{i1} = 0$ when $i \neq 1$) is used to simplify the formula.

When O₃ deposits onto the leaf surface, it has to pass through the quasi-laminar sublayer above the leaf surface at first, then diffuses into the stomata and is finally destroyed inside the stomatal pores reflected by negligible mesophyll resistance. Alternatively, O₃ can deposit onto the leaf cuticle if the leaf is dry, or it is absorbed by the wet skin on leaf surface. So the leaf
 30 surface resistance r_{veg} for each layer can be calculated as

$$r_{veg} = r_b + \frac{1}{\alpha/(r_{stm} + r_{mes}) + (1 - f_{wet})/r_{cut} + f_{wet}/r_{ws}} \quad (3)$$



here r_b is the quasi-laminar boundary layer resistance over the leaf surface, which depends on molecular diffusivity and horizontal wind speed. r_{stm} is the stomatal resistance which is calculated from the evapotranspiration rate in SOSAA, r_{mes} ($= 1 \text{ s m}^{-1}$) is the mesophyll resistance, r_{cut} ($= 10^5 \text{ s m}^{-1}$) is the cuticular resistance and r_{ws} ($= 2000 \text{ s m}^{-1}$) represents the uptake on leaf wet skin. α is a correction factor reflecting the leaf shape. For needle leaves, the uptake on stomata, cuticles and wet skins occur on all sides of leaves, so α is set to 1.0. While for broad leaves, the stomatal uptake only happens on one side, so α is 0.5. Canopy wetness is represented by the fraction of wet skin f_{wet} which is determined by RH according to Lammerl (1999):

$$f_{wet} = \begin{cases} 1 & 0.9 \leq \text{RH} \\ \frac{\text{RH}-0.7}{0.2} & 0.7 \leq \text{RH} < 0.9 \\ 0 & \text{RH} < 0.7 \end{cases} \quad (4)$$

The threshold 70% is suggested in Altimir et al. (2006).

10 In the model the O_3 concentration is calculated for each layer by the continuity equation

$$\frac{\partial[\text{O}_3]}{\partial t} = \frac{\partial}{\partial z} \left(K_t \frac{\partial[\text{O}_3]}{\partial z} \right) - \frac{F}{\Delta z} \quad (5)$$

where K_t is the turbulent eddy diffusivity for O_3 and the first term on the right-hand side represents the vertical mixing of O_3 . Δz is the layer height. LAI effect is already included in the calculation of deposition velocity (Eq. (2)), hence it is not explicitly multiplied in this equation. In addition, the O_3 turbulent flux (F_t) in the model can be obtained as

$$15 \quad F_t = K_t \frac{\partial[\text{O}_3]}{\partial z} \quad (6)$$

with positive values representing downward flux.

The diagram of the resistance analogy parameterisation method described above is shown in Fig. 1. All the symbols are also explained and listed in Table 1.

2.4 Model setup

20 In this study the newly implemented O_3 dry deposition module has been applied to simulate the time period from Aug 1st to Aug 31st 2010 (Julian day 213 to 243). The model column domain was set from 0 m at ground surface up to 3000 m with 51 layers logarithmically configured, including the whole planetary boundary layer and part of the free atmosphere on top of it. We also constrained the model with the site-specific vegetation cover properties as presented before in section 2.1. The overstory layers only included needle-leaf part of Scots pine trees above ~ 0.3 m. Below that there was the understory vegetation and ground surface. Since the understory consisted of vegetation with leaves instead of needles, we set $\alpha = 0.5$ for the understory vegetation same as that for broadleaved species. In order to secure a more accurate representation of canopy wetness which was also relevant to the calculation of the O_3 deposition velocity, RH values inside the canopy were constrained with the measured data.

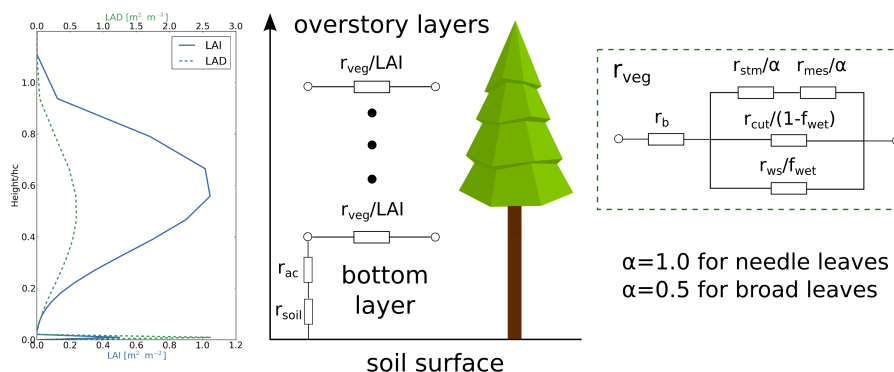


Figure 1. Vertical profiles of all-sided LAI (leaf area index) and LAD (leaf area density), as well as the diagram of resistance analogy method used in the O_3 dry deposition model. The overstory layers and the bottom layer are considered separately. The bottom layer includes the understory vegetation and soil surface. r_{ac} is the resistance representing the turbulent transport from the reference height of the understory vegetation to the soil surface. r_{soil} is the soil resistance, r_{veg} represents the resistance to vegetation leaves, which is plotted on the right-hand side in details. Here r_b is the quasi-laminar boundary layer resistance above the leaf surface, r_{stm} is the stomatal resistance and r_{mes} is the mesophyll resistance. r_{cut} is the cuticular resistance, r_{ws} is the resistance to wet skin. f_{wet} is the wet skin fraction. α is a correction factor reflecting the leaf shape, which is 1.0 for needle leaves and 0.5 for broad leaves. All the variables are defined for each layer. Note that here LAI is the all-sided leaf area index for each layer. The symbols are also explained in the text and Table 1.

In addition, to secure a realistic simulation of O_3 in a column model like SOSAA we also forced the model's O_3 concentration at 23 m towards the observed O_3 concentration to account for the advection of air masses (Fig. 2b). The O_3 concentrations at other heights inside the canopy were calculated from Eq. (6).

3 Results and discussion

5 3.1 Micrometeorology

The simulated month was warm and dry with little precipitation. Moreover, the temperature decreased dramatically in the middle of the month. In the first half of month (Aug 1st to Aug 15th) the average temperature at 23 m was 19.0 °C, while it dropped to 12.1 °C in the second half of month (Aug 16th to Aug 31st). The time series of temperature especially this transition were well predicted by the model (Fig. 2a). RH varied inversely with air temperature. Its average value increased only slightly from 66.0% in the first half of the month to 69.3% in the second half. However, a dramatic increasing of daily mean RH values from 49.3% to 73.5% occurred between Aug 20th and Aug 21st. The combination of the dry weather and the large variation of temperature provided a good sample for verifying the O_3 dry deposition module. It was also interesting to study this featured time period with hot and dry climate which probably represented a future trend at this boreal forest site (Williams et al., 2011).



Table 1. Table of symbols

symbol	value	unit	description
h_c	18	m	canopy height
u_*		m s^{-1}	friction velocity at canopy top
F		ppbv m s^{-1}	O_3 deposition flux
F_t		ppbv m s^{-1}	O_3 turbulent flux
K_t		$\text{m}^2 \text{s}^{-1}$	turbulent eddy diffusivity for O_3
$[\text{O}_3]$		ppbv	O_3 concentration
V_d		m s^{-1}	O_3 dry deposition velocity
r_{veg}		s m^{-1}	leaf surface resistance
r_{soil}	600	s m^{-1}	soil resistance
r_{ac}	1	s m^{-1}	resistance of turbulent transport from the reference height of the understory vegetation to the soil surface
r_b		s m^{-1}	quasi-laminar boundary layer resistance over leaf surface
r_{stm}		s m^{-1}	stomatal resistance
r_{mes}	1	s m^{-1}	mesophylllic resistance
r_{cut}	10^5	s m^{-1}	cuticular resistance
r_{ws}	2000	s m^{-1}	wet skin resistance
α		-	a correction factor reflecting the leaf shape
f_{wet}		-	fraction of wet skin

Figure 3 showed the comparison results between simulated and measured horizontal wind speed and friction velocity (u_*) which both were essential for the turbulent transport above and within the canopy as well as for the calculation of the quasi-laminar boundary layer resistance of leaves (r_b) at each canopy layer. Figure 3a showed the good agreement between modelled and measured monthly-mean horizontal wind speed profiles during both daytime and nighttime. The wind speed decreased quickly inside the canopy due to canopy drag, then changed little below $0.5 h_c$ until near the surface where wind speed varied logarithmically to zero on the surface. The simulated turbulent mixing above and within the canopy was evaluated by comparisons of the modelled and measured friction velocity (Fig. 3b, 3c and 3d). The model reproduced the diurnal cycle but overestimated the nighttime values by $\sim 0.05 \text{ m s}^{-1}$ in average at the canopy top (Fig. 3c). Below the canopy crown at $\sim 3 \text{ m}$, u_* was underestimated by $\sim 0.02 \text{ m s}^{-1}$ at nighttime and $\sim 0.05 \text{ m s}^{-1}$ at daytime (Fig. 3d). The discrepancy was likely due to the limitation of representing the real heterogeneous dynamics by a 1D model with homogeneous canopy configuration.

3.2 PAR above and below the canopy crown

Photosynthetically active radiation (PAR) plays an important role in stomatal exchange which determines to a large extent the daytime vegetation uptake. The PAR on top of the canopy was calculated directly from the input incoming short wave radiation

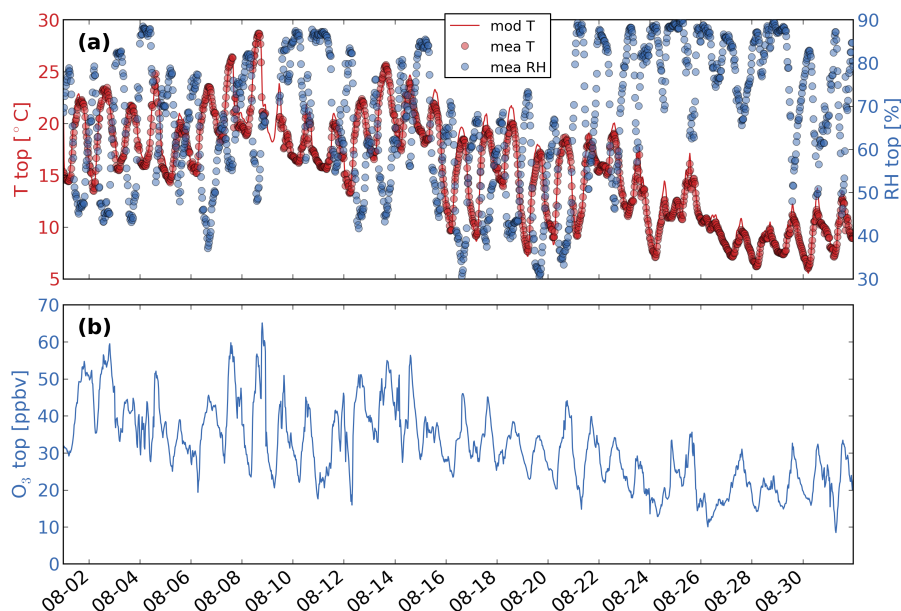


Figure 2. (a) Modelled (solid line) and measured (dots) time series of air temperature (red) and the measured ambient relative humidity (blue) at canopy top. (b) Gap-filled measured O₃ concentration (blue) at canopy top. The time period is August, 2010.

with a daytime maximum of about 250–300 W m⁻² during the simulation month. Inside the canopy, PAR was calculated by considering the absorption, reflection and scattering effects of canopy leaves (Sogachev et al., 2002). The comparison between modelled and observed PAR at ~0.6 m below the canopy crown was shown in Fig. 4. The monthly mean diurnal cycle of attenuated PAR below the canopy crown in the model was consistent with the observation except two missing peaks at daytime (Fig. 4b). These two peaks in the measurement were the consequence of direct exposure of PAR sensors to incoming solar radiation. Such situation always occurred when point-wise measurements were compared with a model assuming a homogeneous forest canopy.

3.3 Energy balance at canopy top

The monthly mean diurnal cycles of sensible heat flux, latent heat flux, net radiation and soil heat flux, were shown in Fig. 5 in order to verify the simulated energy balance in this study. The upward energy flux or the loss of surface energy was represented by positive values. During daytime, the soil and canopy lost energy by heat fluxes and gained energy mainly from net incoming solar radiation. At night, the surface lost energy by net upward long wave radiation with an average rate of ~33 W m⁻², which was partly compensated by ~20 W m⁻² downward energy from transport of warmer air.

During the simulation period the modelled diurnal cycles of energy fluxes agreed well with the observation, although, for example, the latent heat flux was slightly underestimated by ~30 W m⁻² during daytime. In the afternoon from 14:00 to 20:00 the sensible heat flux was underestimated by ~20 W m⁻². This could be explained by the underestimation in net radiation.

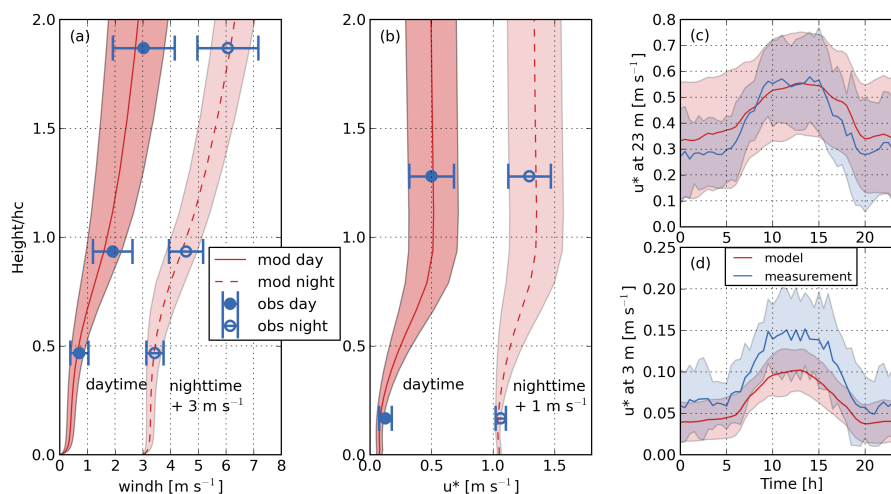


Figure 3. Modelled (red solid line for daytime, red dashed line for nighttime) and measured (blue solid circle for daytime, blue empty circle for nighttime) profiles of horizontal wind speed (windh) (a) and friction velocity (u^*) (b). Nighttime values are added by 3 and 1 m s^{-1} for windh and u^* for clarity, respectively. The ranges of ± 1 standard deviation of modelled and measured data are marked as shades and errorbars. The height is normalised by canopy height h_c . The monthly-mean diurnal cycles of modelled (red) and measured (blue) friction velocity at 23 m and 3 m are shown in (c) and (d). The ranges of ± 1 standard deviation are marked as shades in the same colours.

However, the modelled values were generally within the one standard deviation of the observation. The agreement between modelled and measured latent heat flux also indicated that the stomatal exchange, which controlled the latent heat flux and was directly related to the stomatal resistance of O_3 and many other gaseous compounds, was realistically simulated as a function of the meteorological drivers.

5 3.4 O_3 fluxes at the canopy top

The modelled time series of O_3 turbulent flux and its diurnal cycle were compared with the measurement data at the canopy top (Fig. 6). The simulated O_3 turbulent flux was calculated from the O_3 concentration gradient and the turbulent eddy diffusivity at 23 m.

In general, the modelled flux showed a good agreement with the observation especially in the second half of month (Fig. 6a). Large discrepancies mostly occurred in the first half of month which was warm and dry. On the first 3 days of the month, the O_3 turbulent flux was overestimated by the model. At noon on some days (e.g., Aug 9th, 12th, 13th, 14th, 27th, 30th), the model was not able to predict the observed high peaks of O_3 turbulent fluxes. However, the agreement between the simulated and measured monthly-mean diurnal cycles of O_3 turbulent fluxes was promising.

Figure 7 showed the correlation between the simulated and measured O_3 turbulent fluxes at the canopy top for different humidity conditions at daytime and nighttime, separately. Previous studies showed that in pine forest RH could enhance both stomatal and non-stomatal O_3 uptake (Lamaud et al., 2002; Altimir et al., 2006; Rannik et al., 2012), especially during night-

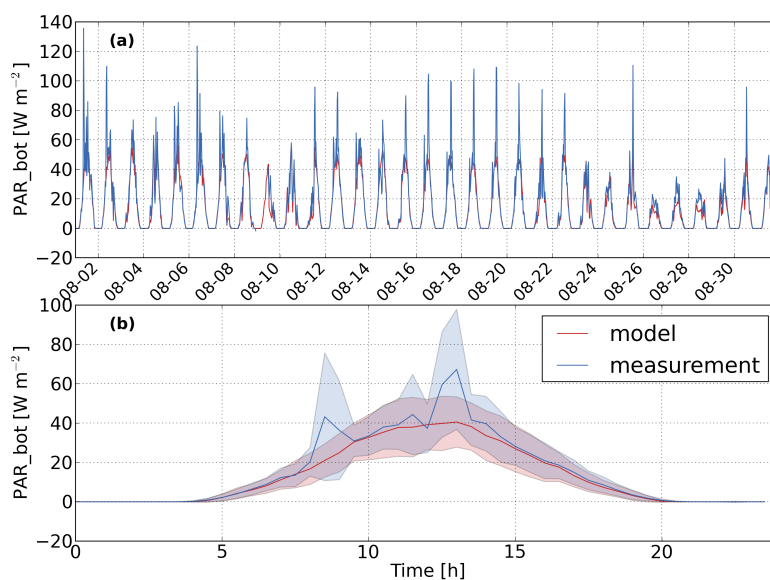


Figure 4. (a) Time series of PAR at 0.6 m from model (red) and measurement (blue) in August, 2010. (b) The monthly averaged diurnal cycle of time series in (a) for model (red) and measurement (blue). The range of ± 1 standard deviation is marked by the shade with the same colour.

time (Rannik et al., 2012). Hence in order to further analyse the impacts of RH, the data were separated into different groups according to daytime and nighttime as well as RH measured at 23 m, representing the daytime with high humidity condition (DH), daytime with low humidity condition (DL), nighttime with high humidity condition (NH) and nighttime with low humidity condition (NL). The data points were considered as daytime when the sun elevation angle was larger than 10° and as nighttime when the sun elevation angle was smaller than 0° . The RH threshold value was set to 70% referring to previous studies (Altimir et al., 2006; Rannik et al., 2012).

The overall R^2 between the modelled and measured O_3 turbulent fluxes for the whole dataset was 0.53. Among the four individual datasets under different conditions, the best prediction by the model occurred for the NH data points with R^2 of 0.36, followed by the condition DH with R^2 of 0.30, both of them were under high humidity conditions. While under low humidity conditions, the correlation with the measurement data was much lower than that for the high humidity conditions. The R^2 of the condition NL was the smallest (0.10) (Fig. 7 and Table 2). This indicated the difficulty of simulating the O_3 turbulent flux in weak turbulent and low humidity conditions at nighttime. Rannik et al. (2009) revealed that the nighttime O_3 turbulent flux were affected by vertical advection of O_3 . Therefore, when wet skin uptake was small for the condition NL, the vertical advection could play a more crucial role in O_3 turbulent flux than deposition. On the other hand, the observed data points in condition NL were more dispersed compared to other conditions which indicated larger random errors induced in measurement. However, when the surface was wetter, the simulated nocturnal O_3 turbulent fluxes correlated much better with

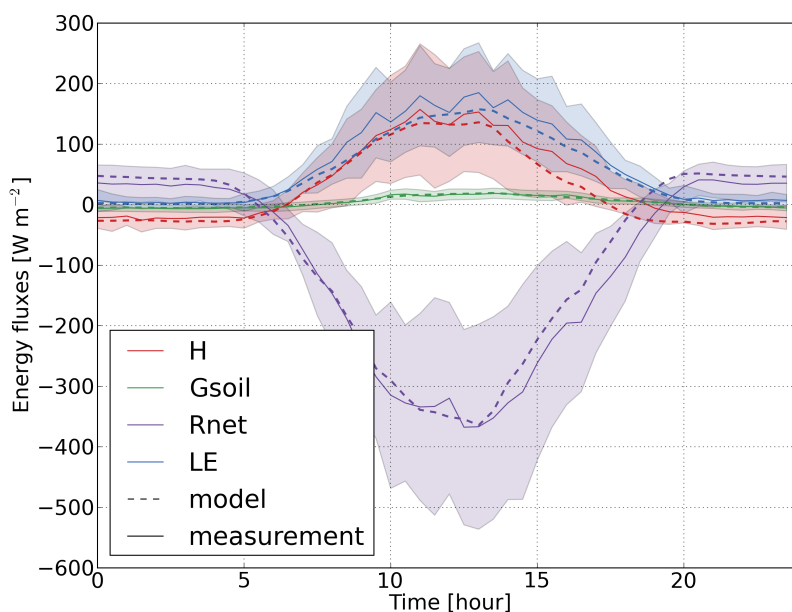


Figure 5. The monthly averaged diurnal cycle of different energy flux terms at canopy top (23 m above the ground) for model (dashed lines) and measurement (solid lines), including sensible heat flux (H, red line), soil heat flux (Gsoil, green line), upward net radiation (Rnet, purple line, note the observed Rnet is at 67 m), latent heat flux (LE, blue line). The range of ± 1 standard deviation for measurement data is plotted for every term by the shade with the same colour.

Table 2. The observed ($F_{t,obs}$) and modelled ($F_{t,mod}$) O_3 turbulent fluxes at the canopy top with their one standard deviation ranges, the relative error of model results and the R^2 values are listed for different conditions DH, DL, NH, NL and ALL. D and N represent daytime and nighttime, H and L represent high and low humidity, respectively. ALL is for the whole dataset.

	$F_{t,obs}$	$F_{t,mod}$	$(F_{t,mod} - F_{t,obs})/F_{t,obs}$	R^2
DH	0.147 ± 0.077	0.124 ± 0.052	-15.6%	0.30
DL	0.183 ± 0.089	0.194 ± 0.066	+6.0%	0.21
NH	0.060 ± 0.037	0.069 ± 0.028	+15.0%	0.36
NL	0.027 ± 0.021	0.044 ± 0.022	+60.3%	0.10
ALL	0.124 ± 0.092	0.130 ± 0.079	+4.7%	0.53

the measurement. In addition, the measurement data showed a larger range of variation ($0.0\text{--}0.6 \text{ ppbv m s}^{-1}$) compared to the range in the modelled O_3 turbulent flux ($0.0\text{--}0.4 \text{ ppbv m s}^{-1}$), which implied that the model did not capture the O_3 turbulent flux peaks or the measurement was more scattered due to random errors.

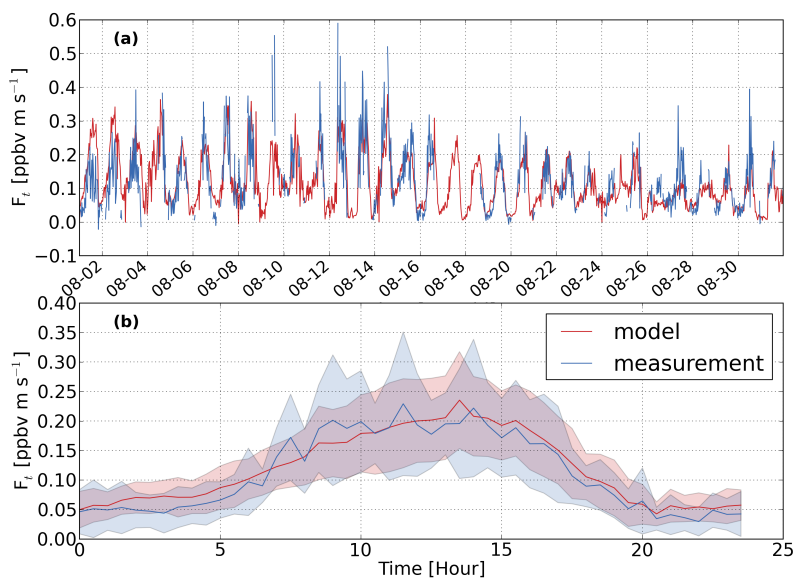


Figure 6. (a) Time series of the simulated (red) and measured (blue) O_3 turbulent fluxes at the canopy top in August, 2010. (b) The monthly averaged diurnal cycles of time series in (a) for the model (red) and measurement (blue). The ranges of ± 1 standard deviation are marked by the shades with the same colours.

Regarding the low R^2 values here, we should consider that the fluxes determined by the eddy-covariance (EC) technique were affected by the stochastic nature of turbulence, revealing random errors of 30 min average fluxes. For the EC measurement the random uncertainty was typically in the order of ten to a few tens of percent. For the O_3 turbulent flux measurement at the same site Keronen et al. (2003) presented the random error statistics, defined as one standard deviation of the random uncertainty of turbulent flux, ranging from about 10 to 40%. Such uncertainty contributed to the data scattering when comparing the modelled and measured fluxes, such as in Fig. 7, and reduced the correlation statistics.

In general, the parameterisation of wet skin fraction (Eq. (4)) and its impact on O_3 non-stomatal removal seemed to represent the O_3 deposition mechanisms inside the canopy well considering the good performance under high humidity conditions. Although the prediction of O_3 turbulent flux with weak turbulence at night under low humidity condition still had large uncertainties (Fig. 7), the simulated average nocturnal O_3 turbulent flux at the canopy top showed a good agreement with the observation (Fig. 6b).

3.5 O_3 concentration profile

In order to evaluate if the good agreement between the observed and simulated O_3 turbulent fluxes at the canopy top also implied a realistic representation of the O_3 concentration inside the canopy, we have conducted an evaluation of the simulated

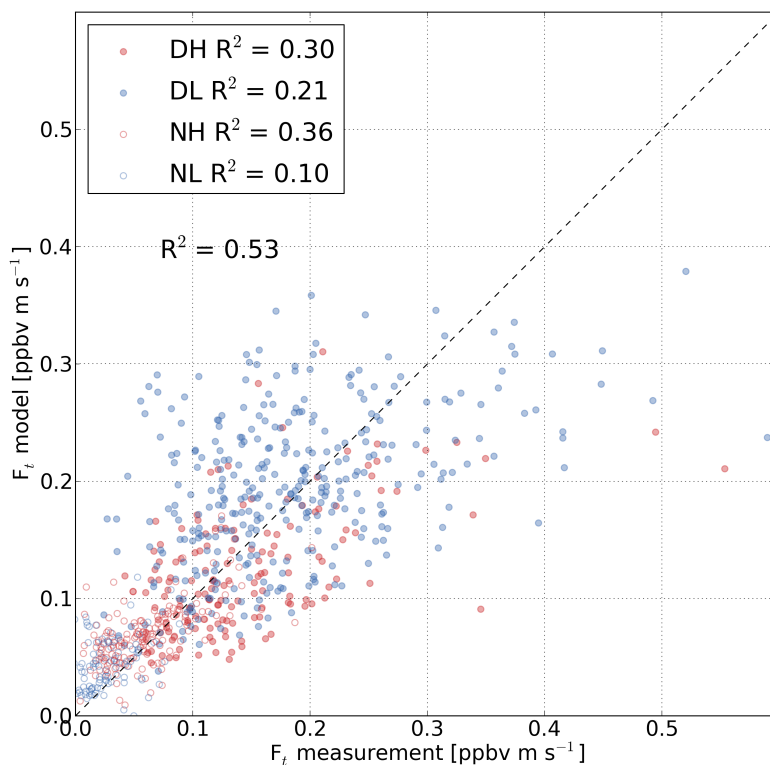


Figure 7. Scattered plot for the modelled versus measured O_3 turbulent fluxes at the canopy top. Four conditions of data points, including daytime points under high (labelled as DH, red solid circle) and low humidity conditions (labelled as DL, blue solid circle), nighttime points under high (labelled as NH, red empty circle) and low humidity conditions (labelled as NL, blue empty circle), are marked separately. The R^2 values are also labelled in the legend for four conditions. The R^2 of the whole dataset is shown below the legend.

in-canopy O_3 concentration profile. The one-month averaged O_3 concentration profiles from model results and measurement were shown in Fig. 8. The huge error bars resulted from the meteorological variations in this month, especially the dramatic transition in the middle of the month (Fig. 2). The average O_3 concentration of the whole month was 31.7 ppbv at 23 m, then decreased gradually inside the canopy to 28.3 ppbv at 4.2 m due to the in-canopy sinks, which were most likely dominated by deposition. Similar vertical gradients were also found for the four different conditions. At night, the turbulent mixing was smaller compared to daytime which inhibited the downward transport of air mass with larger concentration of O_3 into the canopy. Hence the O_3 removal by canopy especially by soil surface resulted in larger gradient of O_3 inside the canopy during nighttime (Fig. 8).

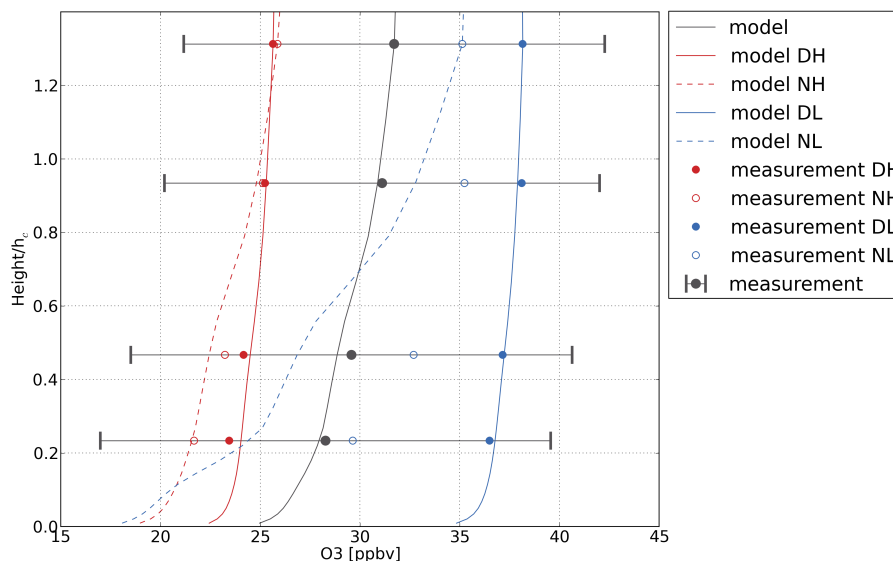


Figure 8. Measured average vertical profiles of O_3 concentration for the whole month (dark grey, the error bars are ± 1 standard deviations) and individual conditions (daytime under high humidity condition, labelled as DH with red filled circle; daytime under low humidity condition, labelled as DL with blue filled circle; nighttime under high humidity condition, labelled as NH with red empty circle; nighttime under low humidity condition, labelled as NL with blue empty circle). Modelled results are plotted as solid lines (daytime) and dashed lines (nighttime) with the same colour as measurement. The height is normalised by the canopy height h_c .

The model results of O_3 concentration profiles showed a good agreement with the observation except the slightly overestimation for the DH condition below ~ 8 m and the apparent underestimation for the NL condition throughout the whole canopy. This was consistent with the model results of the O_3 turbulent fluxes, which showed 15.6% underestimation for the DH condition and 60.3% overestimation for the NL condition (Table 2). In addition, the modelled vertical gradient of O_3 concentration during nighttime at drier condition (NL) was much larger inside the canopy compared to the measured gradient, which implied that the soil deposition was largely overestimated when the soil and dry vegetation surface uptake dominated the overall removal inside the canopy. This also indicates that further investigation is needed for the more precise representation of ground surface deposition at different humidity conditions, including possibly the roles of uptake by the moss layer and soil humus layer.

10 3.6 O_3 flux profile

The modelled vertical profiles of cumulative O_3 deposition flux ($\sum_{k=1}^i F_k$) normalised by the integrated O_3 deposition flux ($\sum_{k=1}^N F_k$) inside the canopy as well as the contributions of different deposition pathways for four different conditions were shown in Fig. 9. For all the four conditions, the O_3 uptake was dominated by soil deposition below $0.2 h_c$ (~ 3.6 m) with little contribution from the understory vegetation via stomatal uptake. From $0.2 h_c$ to $0.8 h_c$ (~ 14.4 m) the uptake on leaf surfaces

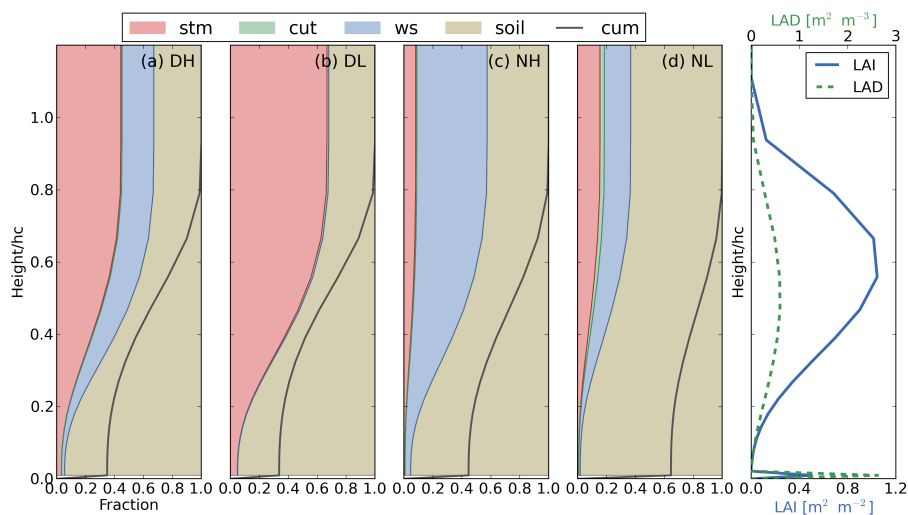


Figure 9. Simulated vertical profiles of cumulative O₃ deposition flux normalised by the integrated O₃ deposition flux at the canopy top (cum, solid black line) for four conditions DH (a), DL (b), NH (c) and NL (d). D and N represent daytime and nighttime, H and L represent high and low humidity, respectively. Shaded areas are the cumulative contribution fractions for different deposition pathways, including stomatal uptake (stm, red), cuticular uptake (cut, green), wet skin uptake (ws, blue) and soil uptake (soil, pale brown). The all-sided LAI profile for each layer and LAD is plotted again here (e). The height is normalised by the canopy height h_c .

increased with height due to dense leaves in the plant crown area. Within this height interval, the stomatal uptake (DL, Fig. 9b), wet skin uptake (NH, Fig. 9c) or both of them (DH, Fig. 9a; NL, Fig. 9d) started to play a significant role in the cumulative O₃ deposition fluxes. Finally, at 0.8 h_c the cumulative contribution of soil deposition was less than 50% except in the NL condition when both the stomatal uptake and wet skin uptake were limited. In all conditions the dry cuticular uptake was minor with a maximum contribution of 3.0% for the NL condition. It should be pointed out that during nighttime at low humidity conditions, the uptake onto wet skin could still exist because the RH inside the canopy at night was usually larger than that at the canopy top. Therefore, although the RH at 23 m was lower than 70%, there could be still quite humid conditions prevailing inside the canopy. At nighttime under high humidity conditions, the wet skin uptake contributed nearly 50% to the total O₃ deposition fluxes (Table 3). This indicated the wet skin uptake relevant to RH played a crucial role at night which was consistent with the results in Rannik et al. (2012). Nearly all of the O₃ uptake occurred below 0.8 h_c (~14.4 m), above this height there only remained small portion of biomass (~7%) providing limited O₃ uptake compared to the total O₃ deposition.

As a result, the simulated non-stomatal contribution to the integrated O₃ deposition flux at the canopy top varied from 33–56% during daytime to 85–92% during nighttime (Table 3). During daytime the sub-canopy layer (lower than 4.2 m according to Launiainen et al. (2013)) including soil surface, contributed about 40% to the integrated O₃ deposition, which was consistent with the results from Launiainen et al. (2013) in which the sub-canopy (lower than 4.2 m) contribution was 35–45% at daytime. At night the contribution increased to around 40% to 65% due to the closed stomata in crown layers. This was much higher than that (25–30%) in Launiainen et al. (2013) (Table 3). The overestimation could result from the underestimation of the



Table 3. The first four columns are the contribution fractions of different deposition pathways (stm as stomatal uptake, wet as wet skin uptake, cut as cuticular uptake, soil as soil surface uptake) in the integrated O₃ deposition flux inside the canopy in the model. The last column is the sub-canopy (below 4.2 m) O₃ turbulent flux ($F_{t,mod}(4.2m)$) compared to the O₃ turbulent flux at the canopy top ($F_{t,mod}$) in the model. Different conditions are listed along the row. D and N represent daytime and nighttime, H and L represent high and low humidity, respectively. ALL is for the whole dataset.

	stm	wet	cut	soil	$F_{t,mod}(4.2m)/F_{t,mod}$
DH	44.3%	22.0%	0.8%	32.9%	39.5%
DL	66.7%	0.0%	1.2%	32.0%	37.8%
NH	8.0%	48.6%	0.8%	42.6%	49.4%
NL	15.5%	18.2%	3.0%	63.4%	67.6%
ALL	47.8%	14.5%	1.2%	36.5%	42.5%

soil resistance, which was difficult to determine in such a complex ground ecosystem. However, among these four different conditions with the same constant soil uptake efficiency, only under the nocturnal dry conditions (NL) there was apparently an overestimation in O₃ uptake and consequently underestimation of the O₃ concentration inside the canopy (Fig. 8). Therefore, we expected that the poor performance for the condition NL also resulted from the limitation of EC measurement technique under weak turbulence near the ground, and the assumption that the resistance r_{ac} between the understory vegetation and ground was not a limiting factor for soil deposition might not hold under certain conditions. On the other hand, Launiainen et al. (2013) studied one month earlier (July 1st to August 4th, 2010) than the time period (August 1st to August 31st, 2010) in this study, so the difference between these two studies could also be due to the meteorological and biological variations during the two summer months. However, the daytime contribution of the sub-canopy layer was consistent, so the difference between the two months could only play a minor effect.

3.7 Chemical removal process

The role of chemical processes in explaining the O₃ removal inside the forest canopy have been discussed in previous studies (e.g., Altimir et al., 2006; Wolfe et al., 2011; Rannik et al., 2012). A study by Wolfe et al. (2011) found that the non-stomatal uptake over a Ponderosa pine stand in the US was associated with additional very reactive BVOCs being present besides the identified ones. On the other hand, Rannik et al. (2012) suggested that the air chemistry provided only minor contribution at SMEAR II. In this study we calculated the time scales of different removal processes to estimate the contribution of air chemistry. Although the time scale might not be a good criteria of chemical influence (Wolfe et al., 2011), it was still acceptable for a first qualitative estimate of the role of in-canopy chemistry on O₃ removal inside the forest canopy.

The average value of measured O₃ flux ($F_{O_3,avg}$) in August, 2010 on top of the canopy was 0.17 ppbv m s⁻¹ at daytime and 0.05 ppbv m s⁻¹ at nighttime whereas the O₃ concentration ([O₃]) inside the canopy was about 32 ppbv during daytime and



26 ppbv at night on average. So the time scale of total O₃ flux (τ_{O_3}) could be obtained from

$$\tau_{O_3} = [O_3] h_c / F_{O_3,avg} \quad (7)$$

which was 3384 s (~1 h) for daytime and 9349 s (~2.5 h) for nighttime. The total O₃ reactivity (y) at 18 m during a similar time period and at the same boreal forest station was calculated by Mogensen et al. (2015), which was $1.58 \times 10^{-5} \text{ s}^{-1}$ and $1.67 \times 10^{-5} \text{ s}^{-1}$ for noon and 2 a.m. at night. If the same values were assumed to be applicable also inside the canopy, the time scale of the O₃ removal by chemistry (τ_{c,O_3}) was

$$\tau_{c,O_3} = y^{-1} \quad (8)$$

which was 63291 s (~18 h) for daytime and 59880 s (~17 h) for nighttime. These estimates showed that the chemical removal accounted for about 5% and 16% of the total O₃ removal within the canopy at daytime and nighttime, respectively. Thus during daytime the chemical removal affected only marginally the O₃ concentration within the canopy as compared to deposition and during the nighttime the effect was somewhat larger. It should be noted that this estimate was based on the current knowledge of air chemistry which could largely underestimate O₃ reactions with oxidised VOCs (Mogensen et al., 2015). Hence the chemical removal of O₃ might be larger than calculated here.

Turbulent transport within the canopy occurred at much shorter time scales than deposition and chemistry. For the same site Rannik et al. (2009, 2015) have estimated the time scale of turbulent transport within the canopy to be in the order of one minute for daytime and about ten minutes for nighttime conditions. This was typically shorter than the deposition time scale and much shorter than the time scale of chemical removal. In addition, the vertical flux was affected only if the chemistry modified the O₃ concentration differentially with height. Therefore the sinks or sources due to chemistry were likely to only introduce concentration change within the atmospheric column that is much higher than the forest layer.

4 Summary

A detailed multi-layer O₃ dry deposition model has been implemented into SOSAA to investigate the O₃ uptake by canopy and soil surface at a boreal forest station SMEAR II. The presented detailed analysis of the O₃ deposition processes for this site was also motivated by the fact that it informed us about the representation of various removal processes, e.g., by the dry and wet cuticle, by stomatal uptake and by the soil surface, which were also involved in the removal of BVOCs and their oxidation products. In this model the fraction of wet skin on canopy leaves was parameterised according to RH values to analyse the potential role of canopy wetness on O₃ deposition for both high and low humidity conditions. Moreover, the multi-layer model also enabled the study of deposition processes inside the canopy and the partitioning of O₃ deposition fluxes between the canopy crown and sub-canopy. In this study, the model has been validated by comparing the modelled and measured O₃ turbulent flux at the canopy top and its concentration profile inside the canopy.

Further investigation has been done through a more in-depth correlation analysis on O₃ turbulent fluxes for nighttime and daytime under high and low humidity conditions. The simulated O₃ turbulent fluxes at the canopy top correlated reasonably



well with the measurement for the whole month with R^2 of 0.53, which was also consistent with the plausible prediction of O_3 concentration profile inside the canopy. The good agreement also applied to the daytime humid and dry as well as nighttime humid conditions (DH, DL and NH) with R^2 of 0.30, 0.21 and 0.36. However, the model was not able to predict high peaks with O_3 turbulent fluxes larger than $0.4 \text{ ppbv m s}^{-1}$. The model also did not capture well the measured O_3 removal for the nocturnal dry condition (NL), in which R^2 was only 0.10 and the O_3 concentration inside the canopy was largely underestimated (Fig. 7 and Table 2). The possible reasons were expected to be the limitation of EC measurement technique under weak turbulence below the canopy crown at nighttime and the excessive ground deposition.

Nearly all of the O_3 uptake occurred below $0.8 h_c$ inside the canopy. During daytime, the contributions of both stomatal uptake (44.3%) and wet skin uptake (22.0%) were significant in the total O_3 uptake under high humidity conditions. While under low humidity conditions the stomatal (66.7%) and soil uptake (32.0%) contributed dominantly the overall canopy deposition. During nighttime, the stomatal uptake contribution (8.0%) was not zero, but was much smaller compared to the wet skin uptake (48.6%) under high humidity conditions. For the low humidity condition at night (NL), the contributions of stomatal uptake (15.5%) and wet skin uptake (18.2%) were similar and both of them were smaller than the soil deposition (63.4%). Therefore, the canopy wetness was considered to play a more crucial role at nighttime, especially under the high humidity condition. In addition, the simulated non-stomatal contributions to the integrated O_3 deposition fluxes were estimated as 55.7%, 33.3%, 92.0% and 84.5% for conditions DH, DL, NH and NL, respectively (Table 3).

The modelled contribution of sub-canopy deposition during daytime (~40%) was consistent with that (35–45%) in Launiainen et al. (2013), but it was much higher at nighttime (about 40–65%) compared to that in the same study (25–30%) (Table 3). This discrepancy at nighttime was most likely due to the overestimation of soil uptake. This also indicated the difficulty of simulating and measuring O_3 deposition at night with weak turbulence (Rannik et al., 2009).

The contribution of O_3 removal by chemical reactions with currently identified BVOCs have also been qualitatively estimated via the analysis of time scales. At daytime, a small fraction of about 5% of O_3 removal resulted from air chemistry compared to deposition. And at nighttime the fraction was about 16%.

This study is the first step to establish a detailed gas dry deposition model in SOSAA. Further implementation will be done for other chemical compounds, especially for BVOCs. This will improve not only the ability of simulating air chemistry and aerosol processes but also our understanding of the mechanisms involved in the removal processes at boreal forest by SOSAA. In addition, it is also interesting to investigate how future climate change might ultimately affect the removal processes of compounds like O_3 and BVOCs for boreal forests.

Author contributions. Putian Zhou implemented the deposition code into SOSAA, made the simulation runs, analysed the results and wrote the main part of this manuscript. Laurens Ganzeveld provided and developed the deposition code, suggested the concepts of manuscript structure, contributed the micrometeorology part and the discussions related to O_3 fluxes. Üllar Rannik contributed the micrometeorology part, the discussions related to O_3 flux measurements and the discussions in chemical removal processes. Luxi Zhou contributed implementing the deposition code into SOSAA and configuration of simulation runs. Rosa Gierens contributed the configuration of meteorology part in SOSAA and configuration of simulation runs. Ditte Taipale contributed the discussions related to air chemistry and site description.



Ivan Mammarella contributed discussions related to O₃ flux measurements. Michael Boy provided SOSAA code and the main concept and structure of this manuscript.

Acknowledgements. This work was supported by Maj ja Tor Nessling funding, the Academy of Finland (projects 1118615 and 272041), CRAICC (Cryosphere-atmosphere interactions in a changing Arctic climate), eSTICC (eScience tools for investigating Climate Change in Northern High Latitudes) and FCoE (The Centre of Excellence in Atmospheric Science - From Molecular and Biological processes to The Global Climate). This work was also supported by institutional research funding (IUT20-11) of the Estonian Ministry of Education and Research. The authors also wish to acknowledge CSC - IT Center for Science, Finland, for computational resources.



References

- Altimir, N., Kolari, P., Tuovinen, J.-P., Vesala, T., Bäck, J., Suni, T., Kulmala, M., and Hari, P.: Foliage surface ozone deposition: a role for surface moisture?, *Biogeosciences*, 3, 209–228, 2006.
- Boy, M., Sogachev, A., Lauros, J., Zhou, L., Guenther, A., and Smolander, S.: SOSA—a new model to simulate the concentrations of organic vapours and sulphuric acid inside the ABL – Part 1: Model description and initial evaluation, *Atmos. Chem. Phys.*, 11, 43–51, 2011.
- 5 Boy, M., Mogensen, D., Smolander, S., Zhou, L., Nieminen, T., Paasonen, P., Plass-Dülmer, C., Sipilä, M., Petäjä, T., Mauldin, L., Berresheim, H., and Kulmala, M.: Oxidation of SO₂ by stabilized Criegee intermediate (sCI) radicals as a crucial source for atmospheric sulfuric acid concentrations, *Atmospheric Chemistry and Physics*, 13, 3865–3879, doi:10.5194/acp-13-3865-2013, <http://www.atmos-chem-phys.net/13/3865/2013/>, 2013.
- 10 Bäck, J., Aalto, J., Henriksson, M., Hakola, H., He, Q., and Boy, M.: Chemodiversity of a Scots pine stand and implications for terpene air concentrations, *Biogeosciences*, 9, 689–702, 2012.
- Dee, D. P., Uppala, S. M., Simmons, A. J., Berrisford, P., Poli, P., Kobayashi, S., Andrae, U., Balmaseda, M. A., Balsamo, G., Bauer, P., Bechtold, P., Beljaars, A. C. M., van de Berg, L., Bidlot, J., Bormann, N., Delsol, C., Dragani, R., Fuentes, M., Geer, A. J., Haimberger, L., Healy, S. B., Hersbach, H., Hólm, E. V., Isaksen, I., Kållberg, P., Köhler, M., Matricardi, M., McNally, A. P., Monge-Sanz, B. M., Morcrette, J.-J., Park, B.-K., Peubey, C., de Rosnay, P., Tavolato, C., Thépaut, J.-N., and Vitart, F.: The ERA-Interim reanalysis: configuration and performance of the data assimilation system, *Quarterly Journal of the Royal Meteorological Society*, 137, 553–597, doi:10.1002/qj.828, <http://dx.doi.org/10.1002/qj.828>, 2011.
- 15 Fares, S., McKay, M., Holzinger, R., and Goldstein, A. H.: Ozone fluxes in a *Pinus ponderosa* ecosystem are dominated by non-stomatal processes: Evidence from long-term continuous measurements, *Agricultural and Forest Meteorology*, 150, 420–431, 2010.
- 20 Felzer, B. S., Cronin, T., Reilly, J. M., Melillo, J. M., and Wang, X.: Impacts of ozone on trees and crops, *Comptes Rendus Geoscience*, 339, 784–798, 2007.
- Ganzeveld, L. and Lelieveld, J.: Dry deposition parameterization in a chemistry general circulation model and its influence on the distribution of reactive trace gases, *J. Geophys. Res.*, 100, 20 999–21 012, 1995.
- Ganzeveld, L., Lelieveld, J., and Roelofs, G.-J.: A dry deposition parameterization for sulfur oxides in a chemistry and general circulation model, *Journal of Geophysical Research: Atmospheres*, 103, 5679–5694, doi:10.1029/97JD03077, <http://dx.doi.org/10.1029/97JD03077>, 1998.
- 25 Ganzeveld, L., Bouwman, L., Stehfest, E., van Vuuren, D. P., Eickhout, B., and Lelieveld, J.: Impact of future land use and land cover changes on atmospheric chemistry-climate interactions, *Journal of Geophysical Research: Atmospheres*, 115, n/a–n/a, doi:10.1029/2010JD014041, <http://dx.doi.org/10.1029/2010JD014041>, d23301, 2010.
- 30 Ganzeveld, L. N., Lelieveld, J., Dentener, F. J., Krol, M. C., Bouwman, A. J., and Roelofs, G.-J.: Global soil-biogenic NO_x emissions and the role of canopy processes, *Journal of Geophysical Research: Atmospheres*, 107, ACH 9–1–ACH 9–17, doi:10.1029/2001JD001289, <http://dx.doi.org/10.1029/2001JD001289>, 2002a.
- Ganzeveld, L. N., Lelieveld, J., Dentener, F. J., Krol, M. C., and Roelofs, G.-J.: Atmosphere-biosphere trace gas exchanges simulated with a single-column model, *Journal of Geophysical Research: Atmospheres*, 107, ACH 8–1–ACH 8–21, doi:10.1029/2001JD000684, <http://dx.doi.org/10.1029/2001JD000684>, 2002b.
- 35



- Goldstein, A. H., McKay, M., Kurpius, M. R., Schade, G. W., Lee, A., Holzinger, R., and Rasmussen, R. A.: Forest thinning experiment confirms ozone deposition to forest canopy is dominated by reaction with biogenic VOCs, *Geophysical Research Letters*, 31, n/a–n/a, doi:10.1029/2004GL021259, <http://dx.doi.org/10.1029/2004GL021259>, I22106, 2004.
- Guenther, A. B., Karl, T., Harley, P., Wiedinmyer, C., Palmer, P. I., and Geron, C.: Estimates of global terrestrial isoprene emissions using MEGAN(Model of Emissions of Gases and Aerosols from Nature), *Atmos. Chem. Phys.*, 6, 3181–3210, 2006.
- Hari, P. and Kulmala, M.: Station for Measuring Ecosystem-Atmosphere Relations (SMEAR II), *Boreal Environ. Res.*, 10, 315–322, 2005.
- Junninen, H., Lauri, A., Keronen, P., Aalto, P., Hiltunen, V., Hari, P., and Kulmala, M.: Smart-SMEAR: on-line data exploration and visualization tool for SMEAR stations, *Boreal Environment Research*, 14, 447–457, 2009.
- Kampa, M. and Castanas, E.: Human health effects of air pollution, *Environmental Pollution*, 151, 362–367, 2008.
- 10 Keronen, P., Reissell, A., Rannik, Ü., Pohja, T., Siivola, E., Hiltunen, V., Hari, P., Kulmala, M., and Vesala, T.: Ozone flux measurements over a Scots pine forest using eddy covariance method: performance evaluation and comparison with flux-profile method, *Boreal Environ. Res.*, 8, 425–443, 2003.
- Kolari, P., Pumpanen, J., Kulmala, L., Ilvesniemi, H., Nikinmaa, E., Grönholm, T., and Hari, P.: Forest floor vegetation plays an important role in photosynthetic production of boreal forests, *Forest Ecology and Management*, 221, 241–248, 2006.
- 15 Korhonen, H., Lehtinen, K. E. J., and Kulmala, M.: Multicomponent aerosol dynamics model UHMA: model development and validation, *Atmospheric Chemistry and Physics*, 4, 757–771, doi:10.5194/acp-4-757-2004, <http://www.atmos-chem-phys.net/4/757/2004/>, 2004.
- Kulmala, L., Launiainen, S., Pumpanen, J., Lankreijer, H., Lindroth, A., Hari, P., and Vesala, T.: H₂O and CO₂ fluxes at the floor of a boreal pine forest, *Tellus B*, 60, 167–178, doi:10.1111/j.1600-0889.2007.00327.x, <http://dx.doi.org/10.1111/j.1600-0889.2007.00327.x>, 2008.
- Kurpius, M. R. and Goldstein, A. H.: Gas-phase chemistry dominates O₃ loss to a forest, implying a source of aerosols and hydroxyl radicals to the atmosphere, *Geophysical Research Letters*, 30, n/a–n/a, doi:10.1029/2002GL016785, <http://dx.doi.org/10.1029/2002GL016785>, 1371, 2003.
- 20 Kurtén, T., Zhou, L., Makkonen, R., Merikanto, J., Räisänen, P., Boy, M., Richards, N., Rap, A., Smolander, S., Sogachev, A., Guenther, A., Mann, G. W., Carslaw, K., and Kulmala, M.: Large methane releases lead to strong aerosol forcing and reduced cloudiness, *Atmospheric Chemistry and Physics*, 11, 6961–6969, doi:10.5194/acp-11-6961-2011, <http://www.atmos-chem-phys.net/11/6961/2011/>, 2011.
- 25 Lamaud, E., Carrara, A., Brunet, Y., Lopez, A., and Druilhet, A.: Ozone fluxes above and within a pine forest canopy in dry and wet conditions, *Atmospheric Environment*, 36, 77–88, 2002.
- Lammel, G.: Formation of nitrous acid: parameterisation and comparison with observations, Tech. Rep. REPORT No. 286, Max-Planck-Institut für Meteorologie, 1999.
- Launiainen, S., Katul, G. G., Grönholm, T., and Vesala, T.: Partitioning ozone fluxes between canopy and forest floor by measurements and a multi-layer model, *Agricultural and Forest Meteorology*, 173, 85–99, 2013.
- 30 Mammarella, I., Peltola, O., Nordbo, A., Järvi, L., and Rannik, Ü.: An advanced software package for eddy covariance flux calculation for a wide range of instrumentation and ecosystems, *Atmospheric Measurement Techniques Discussions*, doi:doi:10.5194/amt-2015-323, in review, 2016.
- Massman, W. J.: Toward an ozone standard to protect vegetation based on effective dose: a review of deposition resistances and a possible metric, *Atmospheric Environment*, 38, 2323–2337, 2004.
- Mogensen, D., Smolander, S., Sogachev, A., Zhou, L., Sinha, V., Guenther, A., Williams, J., Nieminen, T., Kajos, M. K., Rinne, J., Kulmala, M., and Boy, M.: Modelling atmospheric OH-reactivity in a boreal forest ecosystem, *Atmos. Chem. Phys.*, 11, 9709–9719, 2011.



- Mogensen, D., Gierens, R., Crowley, J. N., Keronen, P., Smolander, S., Sogachev, A., Nölscher, A. C., Zhou, L., Kulmala, M., Tang, M. J., Williams, J., and Boy, M.: Simulations of atmospheric OH, O₃ and NO₃ reactivities within and above the boreal forest, *Atmos. Chem. Phys.*, 15, 3909–3932, 2015.
- Rannik, Ü., Kolari, P., Vesala, T., and Hari, P.: Uncertainties in measurement and modelling of net ecosystem exchange of a forest, *Agricultural and Forest Meteorology*, 138, 244–257, 2006.
- Rannik, U., Mammarella, I., Keronen, P., and Vesala, T.: Vertical advection and nocturnal deposition of ozone over a boreal pine forest, *Atmospheric Chemistry and Physics*, 9, 2089–2095, doi:10.5194/acp-9-2089-2009, <http://www.atmos-chem-phys.net/9/2089/2009/>, 2009.
- Rannik, U., Altimir, N., Mammarella, I., Bäck, J., Rinne, J., Ruuskanen, T. M., Hari, P., Vesala, T., and Kulmala, M.: Ozone deposition into a boreal forest over a decade of observations: evaluating deposition partitioning and driving variables, *Atmospheric Chemistry and Physics*, 12, 12 165–12 182, doi:10.5194/acp-12-12165-2012, <http://www.atmos-chem-phys.net/12/12165/2012/>, 2012.
- Rannik, U., Zhou, L., Zhou, P., Gierens, R., Mammarella, I., Sogachev, A., and Boy, M.: Aerosol dynamics within and above forest in relation to turbulent transport and dry deposition, *Atmospheric Chemistry and Physics Discussions*, 15, 19 367–19 403, doi:10.5194/acpd-15-19367-2015, <http://www.atmos-chem-phys-discuss.net/15/19367/2015/>, 2015.
- Ruckstuhl, K. E., Johnson, E. A., and Miyaniishi, K.: Introduction. The boreal forest and global change, *Philosophical Transactions of the Royal Society of London B: Biological Sciences*, 363, 2243–2247, doi:10.1098/rstb.2007.2196, <http://rstb.royalsocietypublishing.org/content/363/1501/2243>, 2008.
- Seok, B., Helmig, D., Ganzeveld, L., Williams, M. W., and Vogel, C. S.: Dynamics of nitrogen oxides and ozone above and within a mixed hardwood forest in northern Michigan, *Atmospheric Chemistry and Physics*, 13, 7301–7320, doi:10.5194/acp-13-7301-2013, <http://www.atmos-chem-phys.net/13/7301/2013/>, 2013.
- Smolander, S., He, Q., Mogensen, D., Zhou, L., Bäck, J., Ruuskanen, T., Noe, S., Guenther, A., Aaltonen, H., Kulmala, M., and Boy, M.: Comparing three vegetation monoterpene emission models to measured gas concentrations with a model of meteorology, air chemistry and chemical transport, *Biogeosciences*, 11, 5425–5443, 2014.
- Sogachev, A., Menzhulin, G., Heimann, M., and Lloyd, J.: A simple three dimensional canopy – planetary boundary layer simulation model for scalar concentrations and fluxes., *Tellus*, 54B, 784–819, 2002.
- Stocker, T. F., Qin, D., Plattner, G.-K., Tignor, M., Allen, S. K., Boschung, J., Nauels, A., Xia, Y., Bex, V., and Midgley, P. M.: IPCC, 2013: Climate Change 2013: The Physical Science Basis. Contribution of Working Group I to the Fifth Assessment Report of the Intergovernmental Panel on Climate Change, Cambridge University Press, Cambridge, United Kingdom and New York, NY, USA, 2013.
- Wesely, M. L.: Parameterization of surface resistances to gaseous dry deposition in regional-scale numerical models, *Atmos. Env.*, 23, 1293–1304, 1989.
- Wesely, M. L. and Hicks, B. B.: A review of the current status of knowledge on dry deposition, *Atmospheric Environment*, 34, 2261–2282, 2000.
- Williams, J., Crowley, J., Fischer, H., Harder, H., Martinez, M., Petäjä, T., Rinne, J., Bäck, J., Boy, M., Dal Maso, M., Hakala, J., Kajos, M., Keronen, P., Rantala, P., Aalto, J., Aaltonen, H., Paatero, J., Vesala, T., Hakola, H., Levula, J., Pohja, T., Herrmann, F., Auld, J., Mesarchaki, E., Song, W., Yassaa, N., Nölscher, A., Johnson, A. M., Custer, T., Sinha, V., Thieser, J., Povesle, N., Taraborrelli, D., Tang, M. J., Bozem, H., Hosaynali-Beygi, Z., Axinte, R., Oswald, R., Novelli, A., Kubistin, D., Hens, K., Javed, U., Trawny, K., Breitenberger, C., Hidalgo, P. J., Ebben, C. J., Geiger, F. M., Corrigan, A. L., Russell, L. M., Ouwersloot, H. G., Vilà-Guerau de Arellano, J., Ganzeveld, L., Vogel, A., Beck, M., Bayerle, A., Kampf, C. J., Bertelmann, M., Köllner, F., Hoffmann, T., Valverde, J., González, D., Riekkola, M.-L., Kulmala, M., and Lelieveld, J.: The summertime Boreal forest field measurement intensive (HUMPPA-COPEC-2010): an overview



- of meteorological and chemical influences, *Atmospheric Chemistry and Physics*, 11, 10599–10618, doi:10.5194/acp-11-10599-2011, <http://www.atmos-chem-phys.net/11/10599/2011/>, 2011.
- Wolfe, G. M. and Thornton, J. A.: The Chemistry of Atmosphere-Forest Exchange (CAFE) Model - Part 1: Model description and characterization, *Atmospheric Chemistry and Physics*, 11, 77–101, doi:10.5194/acp-11-77-2011, <http://www.atmos-chem-phys.net/11/77/2011/>,
5 2011.
- Wolfe, G. M., Thornton, J. A., McKay, M., and Goldstein, A. H.: Forest-atmosphere exchange of ozone: sensitivity to very reactive biogenic VOC emissions and implications for in-canopy photochemistry, *Atmospheric Chemistry and Physics*, 11, 7875–7891, doi:10.5194/acp-11-7875-2011, <http://www.atmos-chem-phys.net/11/7875/2011/>, 2011.
- Zhang, L., Brook, J. R., and Vet, R.: On ozone dry deposition—with emphasis on non-stomatal uptake and wet canopies, *Atmospheric*
10 *Environment*, 36, 4787–4799, doi:[http://dx.doi.org/10.1016/S1352-2310\(02\)00567-8](http://dx.doi.org/10.1016/S1352-2310(02)00567-8), <http://www.sciencedirect.com/science/article/pii/S1352231002005678>, 2002.
- Zhou, L., Nieminen, T., Mogensen, D., Smolander, S., Rusanen, A., Kulmala, M., and Boy, M.: SOSAA – a new model to simulate the concentrations of organic vapours, sulphuric acid and aerosols inside the ABL – Part 2: Aerosol dynamics and one case study at a boreal forest site, *Boreal Environment Research*, 19 (suppl. B), 237–256, 2014.
- 15 Zhou, L., Gierens, R., Sogachev, A., Mogensen, D., Ortega, J., Smith, J. N., Harley, P. C., Prenni, A. J., Levin, E. J. T., Turnipseed, A., Rusanen, A., Smolander, S., Guenther, A. B., Kulmala, M., Karl, T., and Boy, M.: Contribution from biogenic organic compounds to particle growth during the 2010 BEACHON-ROCS campaign in a Colorado temperate needleleaf forest, *Atmospheric Chemistry and Physics*, 15, 8643–8656, doi:10.5194/acp-15-8643-2015, <http://www.atmos-chem-phys.net/15/8643/2015/>, 2015.